Improvement of Robustness Blind Image Restoration Method Using Failing Detection Process

Ryohei Teranishi and Tomio Goto
Dept. of Computer Science, Nagoya Institute of Technology, Nagoya, Japan
Email: te06re@splab.nitech.ac.jp, t.goto@nitech.ac.jp

Takahiro Nagata
Panasonic Co. Ltd., Osaka, Japan

***Abstract*—Blurring is one of the representative image degradation, and much research has been done on its restoration -. In these studies, the degradation process of the image is modeled by a point spread function (PSF: Point Spread Function) of blurring, and it is possible to recover from one input image by estimating its PSF. However, when noise is mixed into the image due to factors such as the characteristics of the camera, there is still a failure of the image due to PSF estimation error. In this paper, we introduce a ringing removal method using L_0 regularization. We propose a high-performance restoration method that can estimate clear images, and confirm its effectiveness by experiments.**

***Index Terms*—blur, blind deconvolution, image restoration, point spread function**

I. Introduction

One of the main causes of image deterioration is blurring. When restoring images deteriorated by blurring, since the blur PSF is unknown, it is a particularly difficult process to estimate the PSF and the ideal image from one input image. To solve this problem, a method of alternately the repeating PSF estimation and the reconstruction processing of the ideal image estimation has proved successful [1]. However, in recent years, the resolution of image pickup elements has been increasing, and it is necessary to cope with enlarged blurring. In this paper, we consider image restoration for deteriorated images with large blurring.

When the blur function restores an unknown degraded image, it is necessary to estimate PSF and its ideal image using the input image. By alternately repeating PSF and ideal image estimations, results close to the original image can be obtained. However, ringing causes problems such as failure of PSF estimation. Therefore, it is necessary to improve the repair performance. In our proposed method, during the latent image restoration step, total variation regularization [2]-[5] is applied to reduce texture components and noise. In addition, a shock filter [6]-[9] are applied to emphasize the edges to improve PSF estimation performance. The Krishnan *et al.* method, which offers fast processing, is implemented at deconvolution processes, enables high-speed processing. The gradient reliability map is then applied to decrease edges, which are badly affected during PSF estimation, to improve further performance. This is our main proposal, in contrast to our conventional work. Additionally, processing to remove the generated ringing is applied to the ideal image estimation process. In our experiments, the parameters for the thresholding of the gradient distribution are first optimized to improve the recovery performance. Next, we use Sun's test set to validate the proposed method in the objective evaluation. Finally, we evaluate our proposed method objectively and subjectively using actual blurred images.

Manuscript received January 10, 2020; revised July 27, 2020.

II. Image Restration Algorithm

When image blurring in an image is uniform, blurred image b is modeled as the convolution of latent image x and its PSF k as follows,

$$b = x \otimes k + n \tag{1}$$

where n is noise.

In this paper, we restore images using this blur degradation model. Image restoration can be classified as non-blind or blind deconvolution. Non-blind deconvolution is image restoration when a PSF is known, and blind deconvolution is image restoration when a PSF is unknown. Blind deconvolution is a problem of estimating both an ideal image and its PSF from a single degraded image. Generally, we estimate the final PSF by alternately repeating the latent image estimation (x-step) and its PSF counterpart (k-step). We restore the degraded image by performing a final non-blind deconvolution using the estimated PSF.

III. Blind Image Restoration

Blind image reconstruction is a problem of estimating an ideal image and a degraded PSF from single degraded

doi: 10.18178/joig.8.3.85-92

image. In general, it solves the problem of restoring the ideal image from the estimated PSF (x-step) and the problem of estimating PSF from degraded image (k-step), and performs image restoration by alternately performing these steps. The flow of the blind image restoration is shown in Fig. 1.

In our proposed system, x-step is composed of three stages of deconvolution, TV regularization, and shock filter. In addition, k-step performs processing by the differentiation of degraded image, differential and threshold processing of estimated imaginary image, and PSF calculation by conjugate gradient method. Also, in order to cope with large blur, we use multiscale iterative processing like Cho's method. As a flow of this process, the image size is first reduced, and x-step and k-step are alternately repeated while gradually expanding to the original size, and the PSF estimation is repeated for each scale. The initial value of PSF uses 3×3 Gaussian filter. In addition, alternate iterative processing of PSF estimation is done in gray scale. Then, the final deconvolution is performed using the PSF finally obtained by the iterative process.

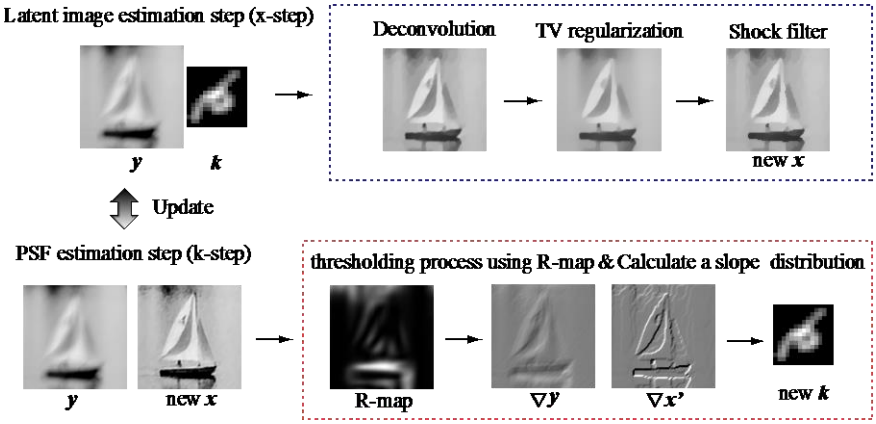

Figure 1. Processing new of our proposed blind deconvolution

A. Latent Image Estimation (x-step)

In the x-step, a restored image x is obtained by deconvolution. However, since noise and ringing occur in the restored image, the texture component of the restored image is removed by TV regularization. Then, a shock filter is applied to the obtained structure component to restore the edge included in the structure component of the image, thereby estimating the ideal image x.

1) Deconvolution

Restore the ideal image x using PSF k obtained by PSF estimation processing. In this research, we use high speed deconvolution using hyper-Laplacian priors proposed by Krishnan *et al.* [10]. This method uses statistical knowledge that the gradient histogram of a natural image obeys a distribution called a heavy tail, and solves the minimization problem of (2) to find an ideal image x. Latent image x is determined by solving the following minimization problem.

$$\mathrm{x} = min_x \sum_{i=1}^{N} \left(\frac{\lambda}{2} (x \otimes k - b)_i^2 + \sum_{j=1}^{J} \left| \left(x \otimes d_j \right)_i \right|^2 \right) \quad (2)$$

where d is a differential filter and $|.|^2$ is a penalty function.

2) Total variation regularization

Total variation regularization [2] is often used to decompose an image into a structure component, which consists of edges and low-frequency components; and a texture component, which consists of small oscillating signals and noise. In the ROF model [2], the evaluation function *F(u)* is minimized to solve an image decomposition as shown in (3):

$$\inf_u F(u) = \sum_{i,j} \left| \nabla_{i,j} \right| + \lambda \sum_{i,j} \left| u_{i,j} - f_{i,j} \right|^2 \quad (3)$$

where $f_{i,j}$ is an input pixel value, $u_{i,j}$ is a computed output pixel value, *i* and *j* are pixel coordinates, and λ is a positive constant. To minimize the evaluation function *F(u)*, we adopt the projection method proposed by Chambolle [3], which is known to be a fast solution. The values, u and $v = f - u$, are the structure and texture components, respectively. The projection method of Chambolle [3] can be expressed by (4) and (5). Where g is an input image, f is an output image, λ is a regularization parameter, τ is a step width, and $p_{x,y}^{(0)} = 0$.

$$p_{x,y}^{(i+1)} = \frac{p_{x,y}^{(i)} + \tau \left\{ \nabla \left(\mathrm{div} p_{x,y}^{(i)} - g/\lambda \right) \right\}_{x,y}}{1 + \tau \left| \nabla \left(\mathrm{div} p_{x,y}^{(i)} - g/\lambda \right)_{x,y} \right|} \quad (4)$$

$$f = g - \lambda \mathrm{div} p_{x,y}^{(i+1)} \quad (5)$$

3) Shock filter

The shock filter [6]-[9] is a filter, which was proposed by Osher and Rudin, that restores or emphasizes edges of an input signal by iterative calculation. The shock filter is represented by the following (6).

$$x_{t+1} = x_t - \mathrm{sign}(\Delta x_t) \| \nabla x_t \| dt \quad (6)$$

where dt is the step-size parameter for the shock filter. The shock filter can adjust the convergence speed according to the value of the step-size dt, and if the dt is 1 or less, it is a filter that can emphasize the edge without causing ringing.

B. PSF Estimation (k-step)

During the k-step, we perform a thresholding process to obtain latent image x estimated during the x-step and to estimate PSF k by solving a minimization problem using a degraded image b and an ideal image x. One specific method for thresholding is dividing the directions of the gradient into four groups: 0°, 45°, 90°, and 135°. We then set the threshold α_g, which is a coefficient of several pixels selected for each group. During the PSF estimation, by using observed image gradient distribution ∇b and predicted latent image gradient distribution ∇x, PSF k is estimated. By minimizing the conjugate gradient method of an energy function as shown in (7), PSF k is estimated thusly.

$$E_k(k) = \left\| \nabla x' \otimes k - \nabla b \right\|^2 + \lambda_k \|k\|^2 \tag{7}$$

IV. Proposed Method

Blind deconvolution occasionally causes a PSF estimation error because of its fine texture components. This may result in failure to restore images. To further improve the restoration performance of blind deconvolution, we add a new process called the "energy function" to the k-step. The energy function represents the degree of convergence of the PSF. If a failure occurs during the iterative process, failure detection is needed to prevent an adverse effect after the iteration, provided there is no breakdown prevention.

A. Gradient Reliability Map (R-map)

(a) Burred image (b) R-map

Figure 2. Example of a gradient reliability map

During the minimization problem for the PSF estimation of our proposed method, strong edges are used. However, those may have a negative influence, owing to noise or narrow signals such as impulse signals. A narrow signal, which is narrower than the blur size, causes a smaller amplitude value when the shock filter emphasizes its edge. This results in an incorrect estimation. Therefore, we apply the gradient reliability map (i.e., R-map) as shown in (8), where $N_h(x)$ is an $h \times h$ window at the center position x. Fig. 2 shows an example of an R-map.

$$r(x) = \frac{\left\| \sum_{y \in N_{h(x)}} \nabla b(y) \right\|}{\sum_{y \in N_{h(x)}} \|\nabla b(y)\| + 0.5} \tag{8}$$

In (8), a thin signal is a numerator with plus and minus cancellation, and r is small. Also, in the flat region, r decreases with the denominator of 0.5. Therefore, if r is large, the reliability of the gradient is high. This r becomes the gradient reliability map (R-map) as it is. Then, a thin signal is excluded by multiplying r' after binarization of r by the gradient of the estimated ideal image. After that, gradient distribution threshold processing is performed. It can be confirmed that the character portion which is one of the thin signals in the deteriorated image is excluded by the gradient reliability map.

B. L_0 Regularization

It is possible to apply ringing removal to natural images by applying a part of the method, which considers L_0 regularized prior distributions of pixel values and image gradients for deblurring. L_0 regularization is a representation of L_0 norm Deconvolution method using hyper-Laplacian [7] is shown to retain fine texture components. However, this method may generate artifacts such as ringing. In contrast, the proposed algorithm with L_0 regularized prior does not generate fine texture components or ringing. Therefore, we propose a method to hold the texture component while reducing the ringing by utilizing the difference between the estimated images.

First, an estimated ideal image I is estimated using a method using hyperlaplacian. Next, the estimated ideal image L_0 is estimated using the proposed algorithm. At this time, only the gradient information $Pt(\nabla x)$ is used.

$$\min_{x,u,g} \|x * k - y\|_2^2 + \mu \|\nabla x - g\|_2^2 + (\lambda \|g\|_0) \tag{9}$$

$$\min_{x} \|x * k - y\|_2^2 + \mu \|\nabla x - g\|_2^2 \tag{10}$$

$$x = \mathcal{F}^{-1}\left(\frac{\overline{\mathcal{F}(k)}\mathcal{F}(y)}{\overline{\mathcal{F}(k)} + } \right) \tag{11}$$

The difference map between the estimated ideal image I and the estimated ideal image L_0 created by (9) to (11) is calculated, and the bilateral filter is used to remove components other than the ringing. Finally, the filtered difference map is subtracted from the estimated ideal image I. This reduces ringing and enables restoration with retention of texture components.

C. Ringing Removal Processing

This section describes the implementation of the ringing removal process. Since ringing may exist in the restored image in the conventional method, it is necessary to remove the ringing. Fig. 3 shows an example of the ringing.

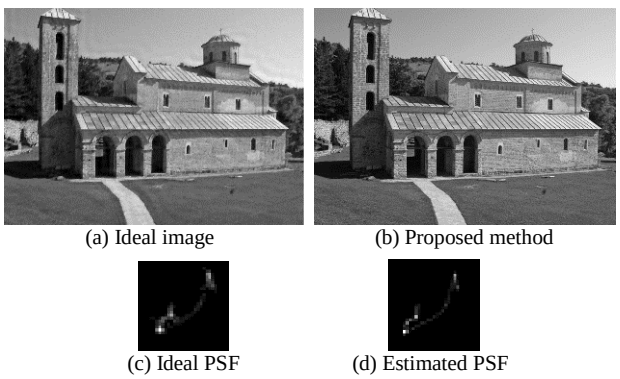

(a) Ideal image (b) Proposed method

(c) Ideal PSF (d) Estimated PSF

Figure 3. The example of ringing

To use the ringing removal process with conventional restoration method, two kinds of implemented methods

are considered. The implemented methods are shown below.

- Add ringing removal after final deconvolution
- Add ringing removal after deconvolution in x-step

Before conducting the above examinations, we will describe the problems of the previous method and their countermeasures. First, there are two problems in the previous method. The first problem is that the estimated ideal image using L_0 regularization may contain salt and pepper noise. The second is that the texture component remains in the difference map filtered by the bilateral filter.

First, how to cope with the first point will be described. Salt and pepper noise refers to noise in which black and white dots spread on an image. This noise is considered to be caused by the fact that the parameters of the ideal image estimation processing by L_0 regularization do not match the image to be restored. Therefore, it is necessary to reduce salt and pepper noise by adjusting the parameters. However, since optimum parameters differ for each image, even if salt and pepper noise is reduced in one image, noise may increase in other images. Therefore, we propose the application of median filter to reduce noise uniformly. Since salt and pepper noise is an outlier, a median filter that takes a median is very effective.

When the median filter is applied, the edge portion becomes dull and the difference between the two estimated ideal images becomes large. However, since the difference map is filtered by the bilateral filter, it is considered that the resulting increased difference is also removed. As described above, there is a second problem that the texture component remains only by the filtering by the bilateral filter. Although it is possible to remove the texture component by applying a bilateral filter strongly, the ringing component is also removed at the same time. Therefore, as a countermeasure against the second problem, a threshold is set in the difference map.

In the proposed method, the above two processes are implemented, and the image quality improvement of the restored image is examined.

V. Experimental Results

A. Objective Evaluation Experiment (Improved Image)

In this section, we show experimental results on the implementation method (proposal 1) in which the ringing removal process is added after the final deconvolution. In this section, the previous research [11] is the conventional method. In this experiment, an evaluation experiment is performed using the test image set for evaluation of blurred image restoration [12] proposed by Sun *et al*. The evaluation using this test set of Sun *et al*. Restores 640 degraded images consisting of 80 ideal images and 8 PSFs, calculates the error rate, PSNR and success rate, and uses them as evaluation values. This evaluation method has been adopted in many articles in recent years. In this experiment, proposal 1 and several related research methods [11]-[16] are compared. Also, in this evaluation, the final non-blind deconvolution is unified to the method of Krishnan [10]. The error rate r is indicated by (12).

$$r = \frac{\|x - \hat{x}_{\hat{k}}\|^2}{\|x - \hat{x}_k\|^2} \tag{12}$$

where x is an ideal image, and $\hat{x}_{\hat{k}}$ is a restored image using the estimated PSF of each method. Also, $\hat{x}_k$ is a restored image using the ideal PSF. As the error rate r approaches 1, it means a better result.

The experimental conditions of proposal 1 are shown in Table I. The optimized value is used for α_g. In the paper by Michaeli *et al.*, if the error rate is less than 5, it is evaluated that restoration is successful, and the same evaluation is made in this paper. Table II shows the results of objective evaluation, and Fig. 4 shows the cumulative error rate that indicates the success rate. The average PSNR and the average error rate are calculated from the average of 640 experimental results, and the maximum error rate indicates the error rate of the image with the worst recovery result. The success rate indicates the proportion of images having an error rate of 5 or less. As shown in Table II, the maximum error rate gave the best results compared to the restoration method of other researchers as well as the conventional method. In addition, although the success rate is inferior to Michaeli's method , the same result as the proposal method is obtained. On the other hand, the average PSNR and the average error rate were inferior to those of the conventional method. However, when compared with other researchers' recovery methods, it can be confirmed that the average PSNR is partially inferior but remains high standards and the average error rate is excellent. From these results, it can be confirmed that proposal 1 is a method for preventing significant deterioration while maintaining the conventional restoration performance. In addition, as shown in Fig. 4, in comparison with the conventional method, proposal 1 shows that the number of high-resolution images with low error rates is small, and the number of images with an error rate of 10 or more is same. On the other hand, when compared with the method of Michaeli *et al.*, proposal 1 has many high definition images, but also many images that are largely broken at the same time. In these results, it can be confirmed that proposal 1 is a high-resolution and robust recovery method, although it is slightly inferior to the conventional method and the method of Michaeli *et al*.

TABLE I. Experimental Parameters for Proposed Method

PSF size			31×31
Iterative number at each scale			5
Latent image estimation process	Deconvolution	λ_d	1500
	TV Regularization	Iterative number	10
		λ_d	20
	Shock Filter	Iterative number	1
		dt	1.0
PSF estimation process	Iterative number		20
	Threshold value		0.05
	α_g		40

TABLE II. EXPERIMENTAL RESULTS OF OBJECTIVE EVALUATIONS

Methods	Average PSNR [dB]	Average Error Ratio	Max Error Ratio	Success Rates [%] ($r \leqq 5$)
Blur input	24.75	5.29	18.23	54.53
Known PSF	31.35	1.00	1.00	100.00
Conventional method [11]	**30.28**	**1.48**	18.72	98.13
Sun *et al*. [12]	30.04	1.68	31.59	96.39
Cho & Lee [13]	26.46	8.18	94.12	73.66
Xu & Jia [14]	29.03	2.57	54.81	92.72
Pan *et al*. [15]	25.40	4.74	22.63	67.81
Michaeli & Irani [16]	28.90	1.98	18.28	**99.06**
proposal 1	30.02	1.58	17.86	98.13
proposal 2	30.01	1.47	**20.30**	97.81

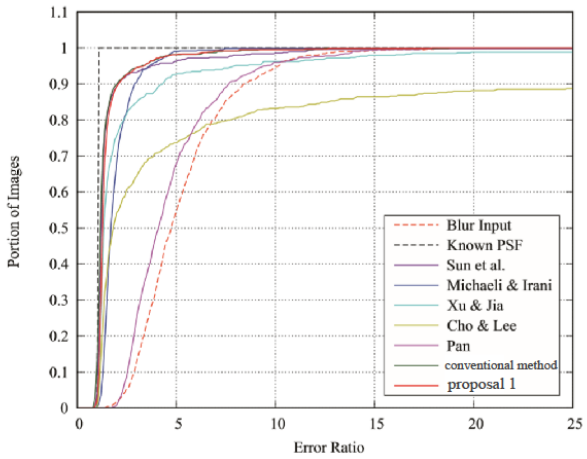

Figure 4. Experimental results of cumulative error rate

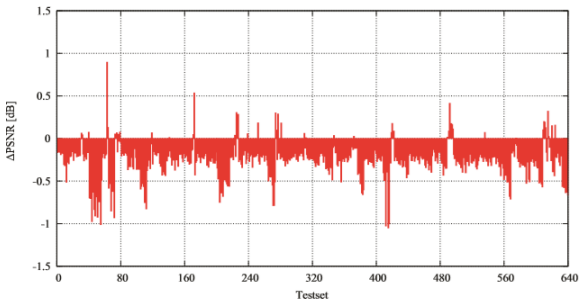

Figure 5. Experimental results of ΔPSNR

Subjective evaluation is also performed focusing on the restoration results of the conventional method and the proposal 1. First, Fig. 5 shows a comparison between PSNR of proposal 1 and PSNR of the conventional method. The horizontal axis in Fig. 5 is the number of test set images, and the vertical axis is Δ PSNR (a value obtained by subtracting PSNR of the conventional method from PSNR of proposal 1). As shown in Fig. 5, the PSNR of proposal 1 is lower than that of the conventional method in many images. However, for some images, it can be confirmed that PSNR is improved by proposal 1. This is because the texture component has been removed rather than the ringing component in an image in which ringing has not occurred. However, since the change amount of PSNR is very small, it is considered that the visual influence in the restored image is small.

The most improved image reconstruction results and estimated PSF in Fig. 5 are shown in Fig. 6. Since the ringing removal of proposal 1 is post-processing, the estimated PSF is the same as that of the conventional method. Error rates r and PSNR are shown below the images.

In Fig. 6, it can be confirmed that the ringing is removed in the portion where the change in pixel value is small, such as the lower part of the image and the sky.

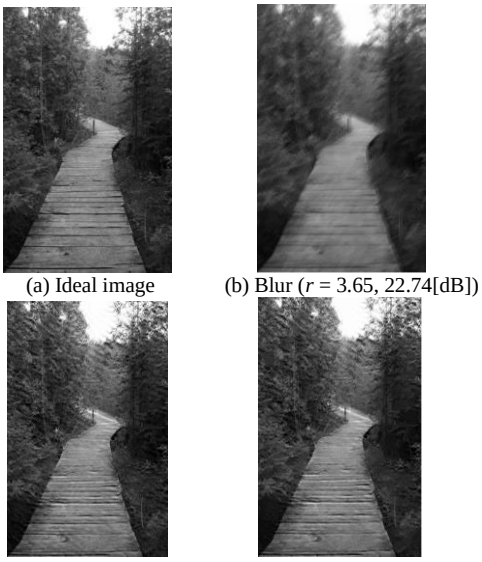

(a) Ideal image (b) Blur (r = 3.65, 22.74[dB])

(c) Conventional method (r = 7.13, 19.60 [dB]) (d) Proposed method (r = 6.05, 20.50 [dB])

Figure 6. Blurred image and restored images (road image)

(a) Ideal PSF (b) Conventional method (c) Proposed method

Figure 7. Estimated PSFs

B. Objective Evaluation Experiment (Degraded Image)

The restoration results of the most degraded image and the estimated PSF are shown in Fig. 8. In Fig. 8, it can be said that the restoration result of the conventional method is a good result because ringing does not occur. On the other hand, it can be confirmed that the restored image of proposal 1 suppresses the texture components of plants and horses. It can be also confirmed that the error rate and PSNR are inferior to the conventional method. However, when compared with the blur-degraded image, visual discomfort can be reduced, and it can be confirmed that good results can be obtained also in the error rate and PSNR. In these results, it can be confirmed that the image quality is degraded due to the suppression of the texture component in the case of the image in which no ringing occurs in proposal 1. On the other hand, in the case of the image in which ringing has occurred, it is considered to be effective because visual discomfort can be reduced.

C. Application Experiment in x-Step

In this section, we show experimental results on an implementation method (proposal 2) in which deconvolution is performed after deconvolution in x-step. In this section, this implementation method is referred to as proposal 2 and prior research [11] is referred to as the conventional method. When the ringing removal process is implemented in the x-step, the ringing removal process is performed only at the final stage because the influence of the component removal becomes large.

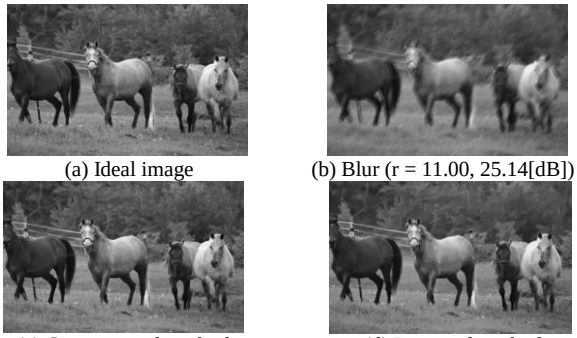

(a) Ideal image (b) Blur (r = 11.00, 25.14[dB])

(c) Conventional method (r = 0.88, 36.22[dB]) (d) Proposed method (r = 1.44, 35.17[dB])

Figure 8. Blurred image and restored images (prairie image)

(a) Ideal PSF (b) Conventional method (c) Proposed method

Figure 9. Estimated PSFs (prairie image)

In this experiment, an evaluation experiment is performed using the test image set for evaluation [12] proposed by Sun *et al*. Similarly, PSNR and error rate *r* are used for the evaluation index. Table III shows the experimental conditions of proposal 2. An optimized value is used for α_g. The results of the objective evaluation are shown in Table II (proposal 2), and the cumulative error rates that indicate success rates are shown in Fig. 10. As Table II shows, proposal 2 achieves better results in average PSNR and average error rate compared to the conventional method. On the other hand, when the results of the maximum error rate and the success rate are compared, proposal 2 has a slightly lower value than the conventional method. However, it can be confirmed that it shows high restoration performance as compared with restoration methods of other researchers. Therefore, it can be confirmed that proposal 2 is an effective method for more images while maintaining the conventional restoration performance. However, when the success rate is compared with the method of Michaeli *et al.* [16], it can also be confirmed that a difference still occurs. This is because part of the components necessary for PSF estimation is removed by the ringing removal processing in proposal 2, and PSF cannot be estimated accurately. On the other hand, in the method of Michaeli *et al.*, there is no major failure, and it is understood that the method is stable for all images.

In addition, as shown in Fig. 10, proposal 2 has many high-resolution images with low error rate and few images with a large error rate of 10 or more when compared with the conventional method. On the other hand, when compared with the method of Michaeli *et al.*, it can be confirmed that although there are many images in which the proposal 2 is largely broken, more high-definition images are also obtained.

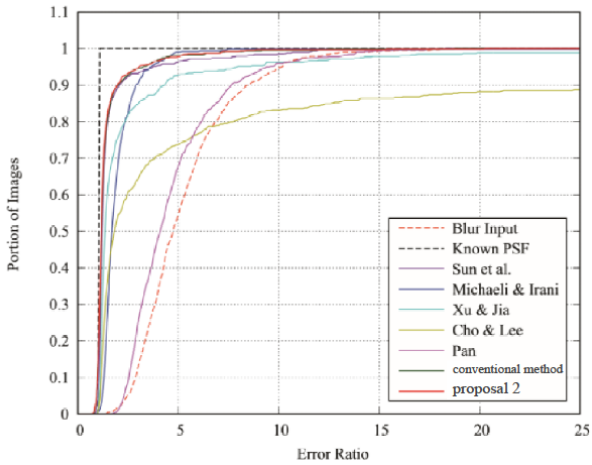

Figure 10. Experimental results of cumulative error rate

TABLE III. EXPERIMENTAL RESULTS OF OBJECTIVE EVALUATIONS

PSF size			31×31
Iterative number at each scale			5
Latent image estimation process	Deconvolution	λ_d	1500
	TV Regularization	Iterative number	10
		λ_d	20
	Shock Filter	Iterative number	1
		dt	1.0
PSF estimation process	Iterative number		20
	Threshold value		0.05, 0.20
	α_g		40

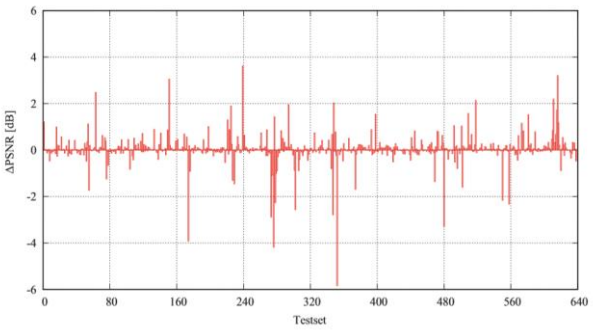

Figure 11. Experimental results of ΔPSNR

Subjective evaluation is performed focusing on the restoration results of the conventional method and proposal 2. First, Fig. 11 shows a comparison between PSNR of proposal 2 and PSNR of the conventional method. Here, the horizontal axis in Fig. 11 is the number of test set images, and the vertical axis is Δ PSNR (the value obtained by subtracting PSNR of the conventional method from PSNR of proposal 2). From Fig. 11, it can be confirmed that some images are significantly

deteriorated compared to the conventional method, but there are also images in which very good results are obtained compared to the conventional method. In addition, 361 images were obtained with better results than the conventional method, and 279 images were degraded compared to the conventional method, so it is considered that the robustness is improved. The most improved image restoration results and estimated PSFs are shown in Fig. 11, and the improved image restoration results and estimated PSFs are shown in Fig. 12 and Fig. 13. Fig. 12, it can be confirmed that in the restored image of proposal 2, most of the ringing present in the entire restored image of the conventional method is removed, and visual discomfort is reduced. This is because the components that adversely affect the PSF estimation are removed by performing the ringing removal processing during the restoration processing. In addition, better results were obtained for both the error rate and PSNR better than both the blurred image and the conventional method. Furthermore, from the estimated PSF of proposal 2, it can also be confirmed that the approximate shape is closer to the ideal PSF than the estimated PSF of the conventional method.

(a) Ideal image (b) Blur (r = 7.10, 18.40[dB])

(c) Conventional method (r = 8.26, 17.57[dB]) (d) Proposed method (r = 3.68, 21.19[dB])

Figure 12. Blurred image and restored images (prairie image)

(a) Michaeli's method (b) Conventional method (c) Proposed method

Figure 13. Estimated PSFs (prairie image)

D. Application Experiment in x-Step

Fig. 14 and Fig. 15 show the result of restoring the most degraded image and the estimated PSF. From Fig. 14, the restored image of proposal 2 is less blurred than the restored image of the conventional method, but ringing due to PSF estimation error occurs around the edge. In addition, the estimated PSF of proposal 2 is broken compared to the estimated PSF of the conventional method. It can be confirmed that the error rate and PSNR are better than those of the blurred image but inferior to the conventional method. This is presumably because no ringing occurred in the restoration by the conventional method, and components necessary for PSF estimation were removed from the estimated ideal image by the ringing removal processing.

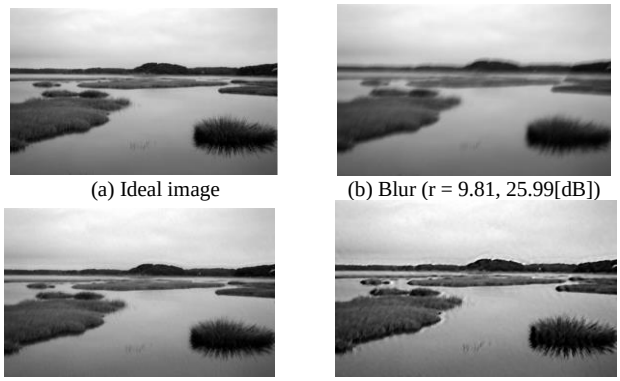

(a) Ideal image (b) Blur (r = 9.81, 25.99[dB])

(c) Conventional method (r = 1.12, 35.15[dB]) (d) Proposed method (r = 4.12, 29.32[dB])

Figure 14. Blurred image and restored images (prairie image)

(a) Michaeli's method (b) Conventional method (c) Proposed method

Figure 15. Estimated PSFs (prairie image)

VI. Conclusion

We proposed a method to remove ringing in the estimated ideal image. After deconvolution processing used in the previous research, ideal image estimation processing using L_0 regularization is performed to calculate a difference map of the two estimated ideal images. The ringing component is extracted from the difference map, and the technique of subtracting from the output image of deconvolution is introduced. The deconvolution using this L_0 regularization can estimate the image without the texture component or the ringing component by using the gradient information of the image. On the other hand, deconvolution using a search table conventionally used can restore fine texture components although ringing may occur. It is possible to remove only the ringing component using these differences. Using this property, we proposed a high-performance reconstruction method that can estimate sharper ideal images by adding ringing removal processing after deconvolution.

The ringing removal process used in the proposed method creates a difference map with the estimated ideal image in the x-step and the estimated ideal image according to the proposed algorithm, and removes only the ringing component with the bilateral filter and the threshold. If ringing removal is applied to all multiscales, not only ringing but also the edge required for PSF estimation will be removed. Therefore, ringing removal is performed only at the final stage of multi-scale.

Conflict of Interest

The authors declare no conflicts of interest associated with this manuscript.

AUTHOR CONTRIBUTIONS

Mr. Teranishi designed and executed the experiments and wrote the manuscript, Mr. Nagata contributed to the concept and helped to write the manuscript, and Dr. Goto is a supervisor and edited the manuscript. All authors reviewed and approved the final manuscript.

ACKNOWLEDGMENT

This work was supported by JSPS KAKENHI Grant Number JP18K11372.

REFERENCES

[1] L. Chen, F. Fang, T. Wang, and G. Zhang, "Blind image deblurring with local maximum gradient prior," in *Proc. IEEE Conference on Computer Vision and Pattern Recognition*, 2019, pp. 1742-1750.
[2] S. J. Osher and E. Fatemi, "Nonlinear total variation based noise removal algorithms," *Physica D*, vol. 60, pp. 259-268, 1992.
[3] A. Chambolle, "An algorithm for total variation minimization and applications," *Journal of Mathematical Imaging and Vision*, vol. 20, no. 1, pp. 89-97, 2004.
[4] T. Goto, M. Ikeyama, and S. Hirano, "contrast enhancement and detailed enhancement method based on non-linear filtering," in *Proc. IEEE International Conference on Consumer Electronics-Taiwan*, 2018.
[5] T. Munezawa and T. Goto, "Noise removal method for moving images using 3-D and time-domain total variation regularization decomposition," *Journal of Image and Graphics*, vol. 7, no. 1, pp. 18-25, 2019.
[6] S. J. Osher and L. I. Rudin, "Feature-Oriented image enhancement using shock filters," *SIAM Journal on Numerical Analysis*, vol. 27, pp. 910-940, 1990.
[7] J. G. M. Schavemaker, M. J. T. Reinders, J. J. Gerbrands, and E. Backer, "Image sharpening by morphological filtering," *Elsevier Pattern Recognition*, vol. 33, no. 6, pp. 997-1012, Jun. 2000.
[8] Y. Sano, T. Mori, T. Goto, S. Hirano, and K. Funahashi, "Super-resolution method and its application to medical image processing," in *Proc. IEEE Global Conference on Consumer Electronics*, 2017, pp. 771-772.
[9] K. Kano, T. Goto, and S. Hirano, "Super-Resolution technique utilizing a non-linear filter for facial images," in *Proc. IEEE Global Conference on Consumer Electronics*, 2018, pp. 535-536.
[10] D. Krishnan and R. Fergus, "Fast image deconvolution using hyper-Laplacian prior," in *Proc. International Conference on Neural Information Processing Systems*, Dec. 2009, pp. 1033-1041.
[11] T. Nagata, S. Motohashi, and T. Goto, "Blind image restoration of blurred images using failing detection process," in *Proc. Global Conference on Signal and Information Processing*, Nov. 2018, pp. 16-20.
[12] S. Cho, L. Sun, and J. Wang, "Edge-Based blur kernel estimation using patch prior," in *Proc. IIEEE International Conference on Computational Photography*, 2013, pp. 1-8.
[13] S. Cho and S. Lee, "Fast motion deblurring," *ACM Transactions on Graphics (SIGGRAPH)*, vol. 28, no. 5, pp. 145:1-145:8, 2009.
[14] L. Xu and J. Jia, "Two-Phase kernel estimation for robust motion deblurring," in *Proc. European conference on Computer Vision*, 2010, pp. 157-170.
[15] J. Pan, Z. Lin, Z. Su, and M. Yang, "Robust kernel estimation with outliers handling for image deblurring," in *Proc. IEEE Conference on Computer Vision and Pattern Recognition*, 2016, pp. 2800-2808.
[16] T. Michaeli and M. Irani, "Blind deblurring using internal patch recurrence," in *Proc. European Conference on Computer Vision*, 2014, pp. 783-798.

Ryohei Teranishi received the B.S. degree from the Department of Electrical and Electronic Engineering, Nagoya Institute of Technology in 2018. He is currently pursuing the M.S. degree from the Department of Computer Science, Nagoya Institute of Technology, Japan. His research interests are signal and image processing and blind image restration.

Takahiro Nagata received the B.S. degree from the Department of Electrical and Electronic Engineering, Nagoya Institute of Technology in 2017, and M.S. degree from the Department of Computer Science in 2019. He is currently working as employee of Panasonic Corporation in Japan. His research interests are signal and image processing and blind image restration.

Tomio Goto (M'01) received the B.S., M.S., and Ph.D. degrees from Nagoya Institute of Technology in 1997, 1999, and 2007, respectively. He is currently an Associate Professor with the Department of Computer Science, Nagoya Institute of Technology, Japan. His research interests include coding of images, non-linear filtering, noise reduction, and super-resolution, as well as most other applications of digital image processing. He is a senior member of the IEEE, IEICE, ITE, and IEEJ in Japan.